Cooperative Simultaneous Localization and Mapping for Pedestrians using Low-Cost Ultra-Wideband System and Gyroscope

Christian Gentner, Markus Ulmschneider, Thomas Jost
German Aerospace Center (DLR)
Institute of Communications and Navigation
Oberpfaffenhofen, 82234 Wessling, Germany
Email: {Christian.Gentner, Markus.Ulmschneider, Thomas.Jost}@dlr.de

***Abstract*—Ultra-wideband (UWB) is a promising technology for positioning systems that has undergone massive research development in recent years. Most UWB positioning systems assume prior knowledge on the positions of the UWB anchors. Without knowing the UWB anchor positions, an accurate position estimate of an UWB tag is difficult. Hence, this paper presents a novel cooperative pedestrian simultaneous localization and mapping (SLAM) algorithm using an UWB positioning system without the necessity to have the prior information on the UWB anchor positions. To obtain accurate estimates of the UWB anchor positions, the estimations of the UWB anchor positions are shared between different mobile units. An increased accuracy of the estimated UWB anchor position relates directly to a more accurate position estimate of the mobile unit position. We evaluate the proposed algorithm based on measurements with multiple mobile units and fixed anchors with unknown positions. The evaluations show that an accurate position estimation of both the mobile units and the anchors is possible without any prior knowledge on the UWB anchor positions.**

I. Introduction

Pedestrian indoor navigation became a widely spread research topic [1]. For outdoor localization, global navigation satellite systems (GNSSs) are well-known and most used technology for positioning. However, inside buildings or in urban canyons GNSS positioning accuracy might be drastically reduced. Hence, different methods and sensor systems are used to support or replace GNSSs [2], [3]. Using wireless local area networks (WLANs) for indoor positioning is a common approach because WLAN infrastructure is widely deployed [4]–[6]. On the other hand, ultra-wideband (UWB) is a promising technology that has undergone massive research development in recent years for positioning systems [7]–[13]. UWB positioning systems use a large bandwidth which reduces the effect of multipath interference and facilitates the determination of times of arrival. Hence, UWB positioning systems promise a solution for indoor positioning. In order to use UWB positioning systems for positioning, UWB anchors have to be placed at known locations. Without knowing the UWB anchor positions, an accurate position estimate of the receiver is difficult or even impossible.

978-1-5386-1647-5/18/$31.00

This paper presents a novel iterative pedestrian localization algorithm using an UWB positioning system without the necessity to have the prior information on the UWB anchor positions. In many indoor scenarios like malls or office buildings, many pedestrians are walking on different trajectories through the scenario. Hence, the task of estimating a map of anchor positions can be assigned to a group of pedestrians which share their estimations. This work builds on and extends the previous work of [14], where we did not consider reusing information on the UWB anchor positions. The proposed algorithm allows to place UWB anchors at arbitrary positions. Accordingly, the novel algorithm has to estimate the positions of the UWB tag and the UWB anchors simultaneously, which can be interpreted as simultaneous localization and mapping (SLAM) with radio signals. In this paper, we consider mobile units which are equipped with an UWB tag and an inertial measurement unit (IMU). Similar to [13], we fuse the distance estimates of the UWB positioning systems with heading information obtained from the IMU. As we are dealing with a relative positioning system, prior information on the initial mobile unit position and moving direction of at least one mobile unit is mandatory to define a local coordinate system. The concept of multiple mobile units allows to obtain an accurate estimate of the UWB anchor positions. An increased accuracy on the estimated UWB anchor positions relates directly to more accurate position estimates of the mobile units positions. Additionally, we derive a map representation of the moved paths. Thus, if the mobile units know their current location, the information of the mapped paths help to estimate the trajectory of further movements. Additionally, revisiting an area enables to correct estimation errors. By assigning the mapping task to a group of collaborating mobile units, who actively or passively collect measurements within the same environment, allows to merge the resulting individual mapped paths to generate a more complete and accurate map of the area.

The positioning algorithm derived in this paper is implemented as a Rao-Blackwellized particle filter (RBPF), where the movement model incorporates the heading information from the IMU. We evaluate the proposed algorithm based on measurements with multiple moving pedestrians each carrying

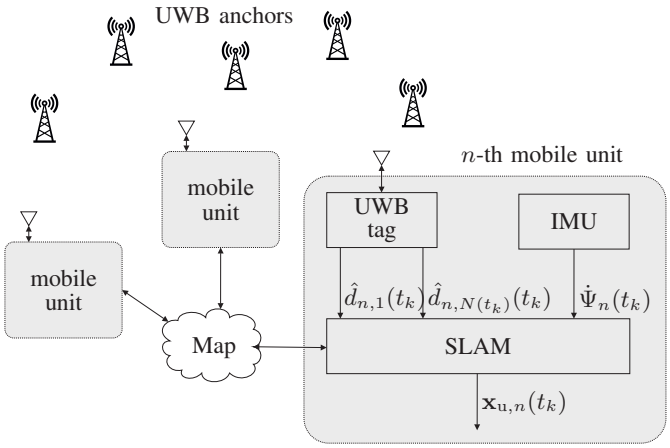

Fig. 1. System model consisting of UWB anchors and mobile units equipped with UWB tags and IMUs.

a mobile unit and fixed anchors with unknown positions in an indoor scenario. The evaluations show that an accurate position estimation of both the pedestrian and the anchors is possible without any prior knowledge on the anchor positions.

The paper is structured as follows. In Section II, we derive the proposed algorithm and describe in Section III the RBPF implementation. Section IV describes the indoor measurement scenario and the evaluation. Finally, Section V concludes the paper.

Throughout the paper, we will use the following notation:

- $(\cdot)^T$ stands for matrix (or vector) transpose.
- All vectors are interpreted as column vectors.
- Vectors are denoted by bold small letters.
- $1:k$ stands for all integer numbers starting from 1 to k, thus $1, 2, \ldots, k$.
- $\mathsf{p}\big(x\big)$ denotes the probability density function of x.

II. Position Estimation

Fig. 1 presents an overview of the available positioning system. The system consists of $N(t_k)$ UWB anchors and $N_m(t_k)$ mobile units. The n-th mobile unit estimates the propagation distances

$$d_{n,i}(t_k) = \|\boldsymbol{r}_{\mathrm{u},n}(t_k) - \boldsymbol{r}_{\mathrm{A},i}(t_k)\| \tag{1}$$

between the n-th mobile unit located at $\boldsymbol{r}_{\mathrm{u},n}(t_k)$ and the anchors located at $\boldsymbol{r}_{\mathrm{A},i}(t_k)$ with $i = 1, \ldots, N(t_k)$. The estimated distances $\hat{d}_{n,i}(t_k)$ of all $N(t_k)$ anchors are used as measurements

$$\mathbf{z}_n(t_k) = [\hat{d}_{n,1}(t_k),\ \ldots\ , \hat{d}_{n,N(t_k)}(t_k)]^T \tag{2}$$

in the localization algorithm with the corresponding standard deviations $\boldsymbol{\sigma}_{z,n}(t_k)$. Please note that the UWB anchors are static in their positions, however, for notational convenience, a time dependence on t_k is introduced here for the anchor positions $\boldsymbol{r}_{\mathrm{A},i}(t_k)$.

The state vector $\mathbf{x}_n(t_k)$ of the n-th mobile unit describing the complete system at time instant t_k is

$$\mathbf{x}_n(t_k) = \left(\mathbf{x}_{\mathrm{u},n}(t_k)^T, \mathbf{x}_{\mathrm{A}}(t_k)^T\right)^T, \tag{3}$$

with the mobile unit state vector $\mathbf{x}_{\mathrm{u},n}(t_k)$ and the anchor state vector $\mathbf{x}_{\mathrm{A}}(t_k)$. The mobile unit state vector $\mathbf{x}_{\mathrm{u},n}(t_k)$ includes the mobile unit's position $\boldsymbol{r}_{\mathrm{u},n}(t_k)$ and velocity $\boldsymbol{v}_{\mathrm{u},n}(t_k)$ with

$$\mathbf{x}_{\mathrm{u},n}(t_k) = \left[\boldsymbol{r}_{\mathrm{u},n}(t_k)^T, \boldsymbol{v}_{\mathrm{u},n}(t_k)^T\right]^T, \tag{4}$$

and the anchor state vector

$$\mathbf{x}_{\mathrm{A}}(t_k) = \left[\boldsymbol{r}_{\mathrm{A},1}(t_k)^T, \ldots, \boldsymbol{r}_{\mathrm{A},N(t_k)}(t_k)^T\right]^T, \tag{5}$$

for the $N(t_k)$ anchor positions $\boldsymbol{r}_{\mathrm{A},i}(t_k)$.

As mentioned before, an IMU is used which provides measurements of the accelerations and turn rates in three dimensions. After preprocessing, the heading change $\dot{\Psi}_n(t_k)$ is used as a control input and is therefore directly integrated into the transition model.

The estimated anchor positions as well as the mapped path of all visited positions are shared between the different mobile units, see Fig. 1. Please note that for simplicity we assume that the merging of the estimated anchor positions and mapped paths is done sequentially. For online merging, further extensions have to be done towards distributed particle filters (PFs), see e.g. [15].

As we consider a dynamic system, the state estimation problem can be seen from a Bayesian perspective: based on measurements, we want to recursively estimate the unknown probability density function (PDF) of the state vector $\mathbf{x}_n(t_k)$ for the mobile unit n. In a recursive Bayesian formulation, this problem can be described as finding the probability distribution

$$\mathsf{p}\big(\mathbf{x}_n(t_{1:k})\,\mathbf{M}|\mathbf{z}_n(t_{1:k})\,\mathbf{u}_n(t_{1:k})\,,\mathbf{x}_n(t_0)\big) = \mathsf{p}\big(\mathbf{x}_{\mathrm{u},n}(t_{1:k})\,,\mathbf{M},\mathbf{x}_{\mathrm{A}}(t_{1:k})|\mathbf{z}_n(t_{1:k})\,\mathbf{u}_n(t_{1:k})\,,\mathbf{x}_n(t_0)\big)\,, \tag{6}$$

with the measurements $\mathbf{z}_n(t_{1:k}) = \left[\mathbf{z}_n(t_1)^T, \ldots, \mathbf{z}_n(t_k)^T\right]^T$, which are the sets of distance measurements for the time instants $t_1, \ldots, t_k$, the control inputs $\mathbf{u}_n(t_{1:k}) = \left[\dot{\Psi}_n(t_1), \ldots, \dot{\Psi}_n(t_k)\right]^T$ and $\mathbf{M}$ defines the mapped path of the mobile units trajectory [16].

Finding the probability distribution in (6) can be regarded as a SLAM problem [17], [18]. It is the joint posterior density of the anchor states, mobile unit state and mapped path given the measurements, the control inputs and the initial states. In case of cooperating mobile units, the initial state on the anchor positions of the n-th mobile unit is obtained from the anchor state estimates of the $n-1$-th mobile unit. We can factorize (6) into

$$\mathsf{p}\big(\mathbf{x}_{\mathrm{u},n}(t_{1:k})\,,\mathbf{M},\mathbf{x}_{\mathrm{A}}(t_{1:k})|\mathbf{z}_n(t_{1:k})\,\mathbf{u}_n(t_{1:k})\,,\mathbf{x}_n(t_0)\big) = \underbrace{\mathsf{p}\big(\mathbf{x}_n(t_{1:k})|\mathbf{z}_n(t_{1:k})\,\mathbf{u}_n(t_{1:k})\,,\mathbf{x}_n(t_0)\big)}_{\text{UWB SLAM}} \tag{7}$$

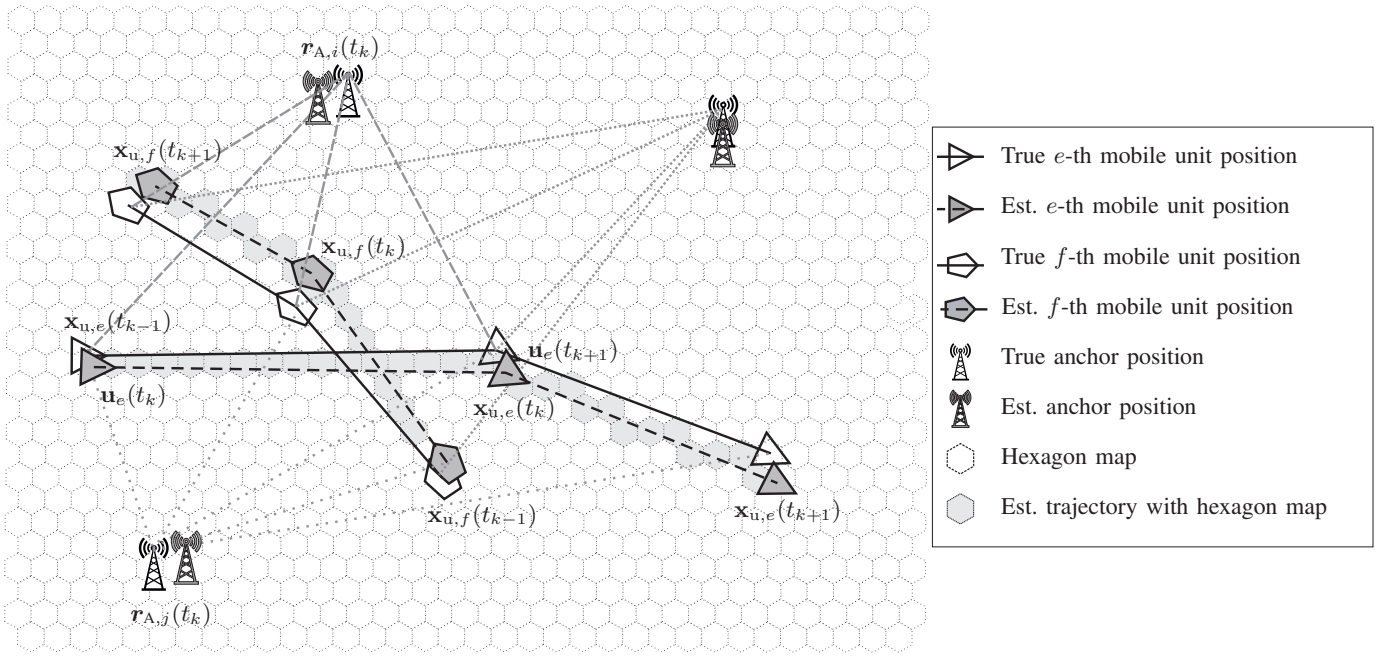

Fig. 2. Overview of the SLAM problem: the mobile units simultaneously estimate their locations, trajectories and the locations of the anchors.

$$\times \underbrace{\mathsf{p}\big(\mathbf{M}|\mathbf{x}_{\mathrm{u},n}(t_{1:k})\big)}_{\text{mapping problem conditioned on the mobile unit state}} \tag{8}$$

where we assume that the map $\mathbf{M}$ only depends on the mobile unit states $\mathbf{x}_{\mathrm{u},n}(t_k)$ as part of $\mathbf{x}_n(t_k)$. (7) and (8) are derived in Section II-A and Section II-B.

Fig. 2 visualizes the SLAM process of this work: the mobile units move through an environment and take distance measurements between a number of anchors with unknown positions and the mobile units. In order to use the distance measurements, the localization algorithm estimates the mobile units and anchor positions simultaneously. The true locations are not known or can not be measured directly. Additionally, the mobile units map the paths represented by the grey hexagons.

A. UWB SLAM

Based on recursive Bayesian filtering, the posterior distribution $\mathsf{p}\big(\mathbf{x}_n(t_{1:k})|\mathbf{z}_n(t_{1:k})\,\mathbf{u}_n(t_{1:k})\,,\mathbf{x}_n(t_0)\big)$ can be obtained recursively by a prediction and an update step. In the prediction step we assume a first-order Markov model and with the transition prior

$$\begin{aligned}&\mathsf{p}\big(\mathbf{x}_n(t_k)|\mathbf{x}_n(t_{k-1})\,,\mathbf{u}_n(t_k)\big)\\ &=\mathsf{p}\big(\mathbf{x}_{\mathrm{u},n}(t_k)|\mathbf{x}_{\mathrm{u},n}(t_{k-1})\,,\mathbf{u}_n(t_k)\big)\\ &\times\prod_{i=1}^{N(t_k)}\mathsf{p}\big(\mathbf{x}_{\mathrm{A},i}(t_k)|\mathbf{x}_{\mathrm{A},i}(t_{k-1})\big)\,.\end{aligned} \tag{9}$$

which depends on the state $\mathbf{x}_n(t_{k-1})$ and the control input $\mathbf{u}_n(t_k)$. The anchor states $\mathbf{x}_{\mathrm{A},i}(t_k)$ are time-invariant, hence, we use the transition prior $\mathsf{p}\big(\mathbf{x}_{\mathrm{A},i}(t_k)|\mathbf{x}_{\mathrm{A},i}(t_{k-1})\big)$ of the i-th anchor

$$\begin{aligned}&\mathsf{p}\big(\mathbf{x}_{\mathrm{A},i}(t_k)|\mathbf{x}_{\mathrm{A},i}(t_{k-1})\big)\\ &\quad=\ \delta\left(\mathbf{x}_{\mathrm{A},i}(t_k)-\mathbf{x}_{\mathrm{A},i}(t_{k-1})\right).\end{aligned} \tag{10}$$

To describe the transition prior $\mathsf{p}\big(\mathbf{x}_{\mathrm{u},n}(t_k)|\mathbf{x}_{\mathrm{u},n}(t_{k-1})\,,\mathbf{u}_n(t_k)\big)$ of the mobile units we consider pedestrians carrying the mobile units and we use the movement model introduced in [19]. During the update step, the measurement $\mathbf{z}_n(t_k)$ is used to correct the prediction based on the measurement likelihood

$$\mathsf{p}\big(\mathbf{z}_n(t_k)|\mathbf{x}_n(t_k)\big)=\prod_{i=1}^{N(t_k)}\frac{1}{\sqrt{2\pi}\sigma_{d,n,i}(t_k)}e^{-\frac{(\hat{d}_{n,i}(t_k)-d_{n,i}(t_k))^2}{2\sigma^2_{d,n,i}(t_k)}}, \tag{11}$$

with the distance estimate $\hat{d}_{n,i}(t_k)$, the propagation distance $d_{n,i}(t_k)$ and the corresponding variance $\sigma^2_{n,d,i}(t_k)$ for the i-th anchor.

B. Path Mapping

Similar to [16], we map the paths based on the previous mobile unit positions. Thus, if we know the current location, we can predict the possible movement based on the mapped paths. In order to estimate and store the probability distribution of mobile units motions as a function of location, we need to partition the space. Equivalently to [20]–[22], we discretize the space into a grid of N_h adjacent hexagons $H_i \in \{H_0, H_1, \ldots, H_i, \ldots H_{N_h-1}\}$, where i uniquely references a position of a hexagon. Fig. 3 shows an example where the walked path is indicated by the black line, the corresponding discretized hexagon map is indicated in grey. We define by $\mathbf{M}$, the time invariant map of the previous mobile units positions

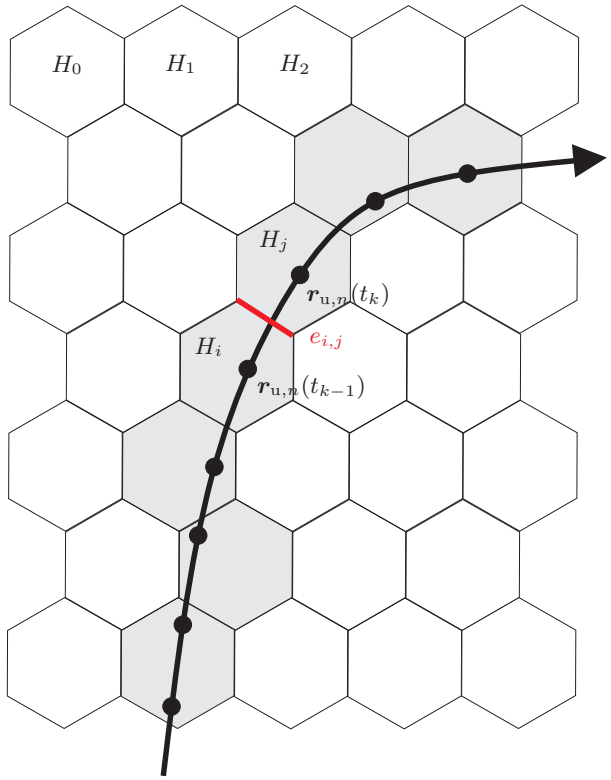

Fig. 3. Mapping the movement by hexagons: the black line indicates the true movement, the grey hexagons shows the mapped movement. Additionally, the figure indicates the movement form $\boldsymbol{r}_{\mathrm{u},n}(t_{k-1})$ to $\boldsymbol{r}_{\mathrm{u},n}(t_k)$, respectively from hexagon H_i to hexagon H_j through the edge $e_{i,j}$.

which can be decomposed as

$$\mathbf{M} = \{\mathbf{m}_0, \mathbf{m}_1, \ldots, \mathbf{m}_i, \ldots, \mathbf{m}_{N_h-1}\} \tag{12}$$

where $\mathbf{m}_i$ is a vector of length 6 denoting the transition probabilities of the hexagon with index i and $\mathbf{m}_i$ is the set of transition probabilities $\{m_i^0, m_i^1, \ldots, m_i^5\}$ across the edges of hexagon H_i. Let us assume the mobile unit moved from hexagon H_i to hexagon H_j through the edge $e_{i,j}$ as depicted in Fig. 3. Thus, we can define the transition probability $m_i^e(t_k)$ of the crossed edge $e_{i,j}$ with

$$m_i^e(t_k) = \mathsf{p}\big(\mathbf{x}_{\mathrm{u},n}(t_k) \in H_j | \mathbf{x}_{\mathrm{u},n}(t_{k-1}) \in H_i\big). \tag{13}$$

where $i \neq j$ and e represents the index of each edge of the hexagon with $e = \{0, 1, \ldots, 5\}$ and $\sum_{e=0}^{5} m_i^e(t_k) = 1$. Hence, by observing the mobile unit states $\mathbf{x}_{\mathrm{u},n}(t_{0:k})$ we can estimate $\mathsf{p}\big(\hat{m}_i^e(t_k)|\mathbf{x}_{\mathrm{u},n}(t_{0:k})\big)$ where $\hat{m}_i^e(t_k)$ denotes the estimate of $m_i^e(t_k)$. Thus, by the division of the space into independent hexagons, the mapping problem can be decomposed into map estimation sub-problems [20], such that we obtain from (8)

$$\mathsf{p}\big(\mathbf{M}|\mathbf{x}_{\mathrm{u},n}(t_{1:k})\big) = \prod_{h=0}^{N_h-1} \mathsf{p}\big(\mathbf{m}_h|\mathbf{x}_{\mathrm{u},n}(t_{0:k})\big)\,. \tag{14}$$

III. RBPF Implementation

The presented recursive Bayesian filter is implemented based on Rao-Blackwellization. The posterior density $\mathsf{p}\big(\mathbf{x}_{\mathrm{u},n}(t_k), \mathbf{M}, \mathbf{x}_{\mathrm{A}}(t_k)|\mathbf{z}_n(t_{1:k})\,\mathbf{u}_n(t_{1:k}), \mathbf{x}_n(t_0)\big)$ of (7) can be written as

$$\begin{aligned}
&\mathsf{p}\big(\mathbf{x}_{\mathrm{u},n}(t_k), \mathbf{M}, \mathbf{x}_{\mathrm{A}}(t_k)|\mathbf{z}_n(t_{1:k})\,\mathbf{u}_n(t_{1:k}), \mathbf{x}_n(t_0)\big)\\
&= \mathsf{p}\big(\mathbf{x}_{\mathrm{u},n}(t_k)|\mathbf{z}_n(t_{1:k}), \mathbf{u}_n(t_{1:k}), \mathbf{x}_{\mathrm{u},n}(t_0)\big)\\
&\quad\times \mathsf{p}\big(\mathbf{x}_{\mathrm{A}}(t_k)|\mathbf{x}_{\mathrm{u},n}(t_k), \mathbf{z}_n(t_{1:k}), \mathbf{x}_{\mathrm{A}}(t_0)\big)\\
&\quad\times \mathsf{p}\big(\mathbf{M}|\mathbf{x}_{\mathrm{u},n}(t_{0:k})\big)\\
&= \mathsf{p}\big(\mathbf{x}_{\mathrm{u},n}(t_k)|\mathbf{z}_n(t_{1:k}), \mathbf{u}_n(t_{1:k}), \mathbf{x}_{\mathrm{u},n}(t_0)\big)\\
&\times \textstyle\prod_{i=1}^{N(t_k)} \mathsf{p}\big(\mathbf{x}_{\mathrm{A},i}(t_k)|\mathbf{x}_{\mathrm{u},n}(t_k), \hat{d}_{n,i}(t_{1:k}), \mathbf{x}_{\mathrm{A},i}(t_0)\big)\\
&\quad\times \mathsf{p}\big(\mathbf{M}|\mathbf{x}_{\mathrm{u},n}(t_{0:k})\big)\,,
\end{aligned}$$

assuming a first-order Markov model. As shown in Fig. 4, the algorithm is based on a superordinate particle filter (superPF) and subordinate particle filters (subPFs). We use PFs to estimate the subspaces representing the anchor states inside a PF. The reason to use a PF instead of a low complexity extended Kalman filter (EKF) is the non-linearity of the measurements in (1). Each particle $j = 1 \ldots N_s$ of the superPF with the state vector $\mathbf{x}_{\mathrm{u},n}^{(j)}(t_k)$ consists of $N(t_k)$ subPFs. Each subPF is represented by the particles $\mathbf{x}_{\mathrm{A},i}^{(j,a)}(t_k)$ with $a = 1, \ldots, N_{P,j,i}$ where $N_{P,j,i}$ stands for the number of particles in the i-th subPF with $i = 1, \ldots, N(t_k)$, estimating $\mathbf{x}_{\mathrm{A},i}^{(j)}(t_k)$.

Consequently, the posterior density $\mathsf{p}\big(\mathbf{x}_{\mathrm{u},n}(t_k), \mathbf{M}, \mathbf{x}_{\mathrm{A}}(t_k)|\mathbf{z}_n(t_{1:k})\,\mathbf{u}_n(t_{1:k}), \mathbf{x}_{\mathrm{u},n}(t_0)\big)$ can be approximated by importance samples, as

$$\begin{aligned}
&\mathsf{p}\big(\mathbf{x}_{\mathrm{u},n}(t_k), \mathbf{M}, \mathbf{x}_{\mathrm{A}}(t_k)|\mathbf{z}_n(t_{1:k})\,\mathbf{u}_n(t_{1:k}), \mathbf{x}_{\mathrm{u},n}(t_0)\big)\\
&\approx \sum_{j=1}^{N_s} w^{(j)}(t_k)\;\delta\left(\mathbf{x}_{\mathrm{u},n}(t_k) - \mathbf{x}_{\mathrm{u},n}^{(j)}(t_k)\right)\,,
\end{aligned} \tag{15}$$

where $w^{(j)}(t_k)$ defines the weight for the j-th particle at time instant t_k with

$$w^{(j)}(t_k) = w_{\mathrm{US}}^{(j)}(t_k) \cdot w_{\mathrm{MP}}^{(j)}(t_k) \tag{16}$$

where $w_{\mathrm{US}}^{(j)}(t_k)$ is the weight of UWB SLAM, see (7), and $w_{\mathrm{MP}}^{(j)}(t_k)$ of the mapped path, see (8). According to [23], $w_{\mathrm{US}}^{(j)}(t_k)$ is defined as

$$\begin{aligned}
w_{\mathrm{US}}^{(j)}(t_k) &\propto \mathsf{p}\big(\mathbf{z}_n(t_k)|\mathbf{x}_{\mathrm{u},n}^{(j)}(t_k), \mathbf{z}_n(t_{k-1})\big)\\
&\propto \prod_{i=1}^{N(t)} \sum_{a=1}^{N_{P,i,j}(t_k)} w_{\mathrm{US},i}^{(j,a)}(t_k)
\end{aligned} \tag{17}$$

where the weight $w_{\mathrm{US},i}^{(j,a)}(t_k)$ of the subPFs at time instant t_k is

$$w_{\mathrm{US},i}^{(j,a)}(t_k) \triangleq \mathsf{p}\big(\hat{d}_{n,i}(t_k)|\mathbf{x}_{\mathrm{u},n}^{(j)}(t_k), \mathbf{x}_{\mathrm{A},i}^{(j,a)}(t_k)\big), \tag{18}$$

assuming Gaussian Kernels $\mathrm{K}(\cdot)$ with weight $w_{\mathrm{US},i}^{(j,a)}(t_k)$, bandwith $\sigma_{\mathrm{K},i}^{(j)}(t_k)$ and

$$\mathsf{p}\big(\mathbf{x}_{\mathrm{A},i}(t_k)|\mathbf{x}_{\mathrm{u},n}^{(j)}(t_k), \hat{d}_{n,i}(t_k)\big) \tag{19}$$

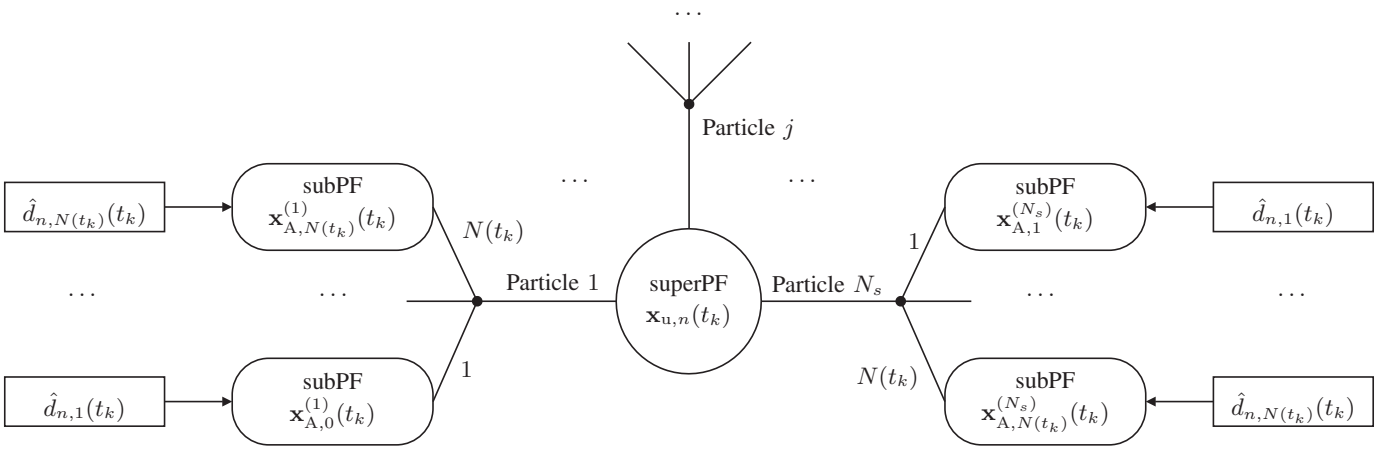

Fig. 4. The algorithm is based on a superordinate particle filter (superPF) and subordinate particle filters (subPFs). Each particle $j = 1 \dots N_s$ of the superPF holds $N(t_k)$ subPFs.

$$\approx \sum_{a=1}^{N_{P,i,j}} w^{(j,a)}_{\mathrm{US},i}(t_k) \cdot \mathrm{K}(\mathbf{x}_{\mathrm{A},i}(t_k) - \mathbf{x}^{(j,a)}_{\mathrm{A},i}(t_k)).$$

Resampling is performed at each time instant to prevent degeneration, hence, (17) and (18) do not depend on the weights $w^{(j)}_{\mathrm{US}}(t_{k-1})$ and $w^{(j,a)}_{\mathrm{US},i}(t_{k-1})$, respectively.

According to [20]–[22], $w^{(j)}_{\mathrm{MP}}(t_k)$ is calculated as

$$w^{(j)}_{\mathrm{MP}}(t_k) = \frac{N^e_i + \alpha^e_i}{N_i + \alpha_i}\,, \tag{20}$$

where the term N^e_i represents the number of transitions for edge e of hexagon H_i and N_i is the sum of all transitions of hexagon H_i with $N_i = \sum_{e=0}^{5} N^e_i$. The terms α^e_i and $\alpha_i = \sum_{e=0}^{5} \alpha^e_i$ represents the a-priori knowledge regarding the number of transitions across the edges of H_i of particle j. Additionally, if the particle crossed multiple hexagons, the weight update is performed for all crossed edges. For a more detailed description about the weight calculation of (20), see [20]–[22].

Similar to SLAM approaches, we estimate, map and reuse anchor positions in this paper. According to (15) and (19), the anchor positions are estimated by a discretized representation of the posterior PDFs, i.e. particle clouds. During the mobile unit's movements, the posterior PDF of the anchor state converges. Hence, many particles of the subPFs are resampled at the same point because the states of the anchors $\mathbf{x}_{\mathrm{A},i}(t_k)$ are time-invariant. Thus, similar to [19], a method to dynamically adapt the number of particles is used, which significantly reduces the computational complexity.

In order to share the estimation of the anchor positions, we need to obtain the PDF $\mathsf{p}\big(\mathbf{x}_{\mathrm{A},i}(t_k)|\hat{d}_{n,i}(t_k)\big)$ of the i-th anchor position $\mathbf{x}_{\mathrm{A},i}(t_k)$ with

$$\begin{aligned}&\mathsf{p}\big(\mathbf{x}_{\mathrm{A},i}(t_k)|\hat{d}_{n,i}(t_k)\big) \qquad (21)\\ &= \int \mathsf{p}\big(\mathbf{x}_{\mathrm{A},i}(t_k)|\mathbf{x}_{\mathrm{u},n}(t_k)\,,\hat{d}_{n,i}(t_k)\big)\mathsf{p}\big(\mathbf{x}_{\mathrm{u},n}(t_k)\big)\mathrm{d}\mathbf{x}_{\mathrm{u},n}(t_k)\,.\end{aligned}$$

Using (15) and (19), we obtain from (21),

$$\begin{aligned}&\mathsf{p}\big(\mathbf{x}_{\mathrm{A},i}(t_k)|\hat{d}_{n,i}(t_k)\big) \qquad (22)\\ &\approx \sum_{j=1}^{N_s} \int \mathsf{p}\big(\mathbf{x}_{\mathrm{A},i}(t_k)|\mathbf{x}_{\mathrm{u},n}(t_k)\,,\hat{d}_{n,i}(t_k)\big) w^{(j)}_{\mathrm{US}}(t_k)\\ &\quad \times \delta\left(\mathbf{x}_{\mathrm{u},n}(t_k) - \mathbf{x}^{(j)}_{\mathrm{u},n}(t_k)\right)\mathrm{d}\mathbf{x}_{\mathrm{u},n}(t_k)\,,\\ &\approx \sum_{j=1}^{N_s} \mathsf{p}\big(\mathbf{x}_{\mathrm{A},i}(t_k)|\mathbf{x}^{(j)}_{\mathrm{u},n}(t_k)\,,\hat{d}_{n,i}(t_k)\big) w^{(j)}_{\mathrm{US}}(t_k)\\ &\approx \sum_{j=1}^{N_s} w^{(j)}_{\mathrm{US}}(t_k) \left(\sum_{a=1}^{N_{P,i,j}} w^{(j,a)}_{\mathrm{US},i}(t_k)\right.\\ &\quad \left.\times \mathrm{K}(\mathbf{x}_{\mathrm{A},i}(t_k) - \mathbf{x}^{(j,a)}_{\mathrm{A},i}(t_k))\right).\end{aligned}$$

Many anchor particle states $\mathbf{x}^{(j,a)}_{\mathrm{A},i}(t_k)$ are similar. Hence, we use a grid based reduction method to reduce the number of particles. Thus, the weights $w^{(j,a)}_{\mathrm{US},i}(t_k)$ are summed up whenever the anchor particle states $\mathbf{x}^{(j,a)}_{\mathrm{A},i}(t_k)$ lie within the same grid.

IV. Evaluations based on Measurements

In this section we evaluate the proposed algorithm based on indoor measurements with 13 fixed anchors and 15 moving pedestrians. The pedestrians are carrying the mobile units which are equipped with an UWB tag, a Xsense IMU (MTI-G-700) and a laptop which stores the IMU and UWB measurement data. We use the so called *Loco Positioning system* produced by *Bitcraze AB*, see *https://www.bitcraze.io/* for our measurements. The *Loco Positioning system* is based on the *Decawave DWM1000* chip and has a nominal accuracy in the decimeter range. For the measurements, the UWB system is configured to a bandwidth of 500 MHz and a carrier frequency of 3.5 GHz. For ranging, we use a two way ranging method, see [14] for details.

Fig. 5 shows the indoor measurement scenario in top view

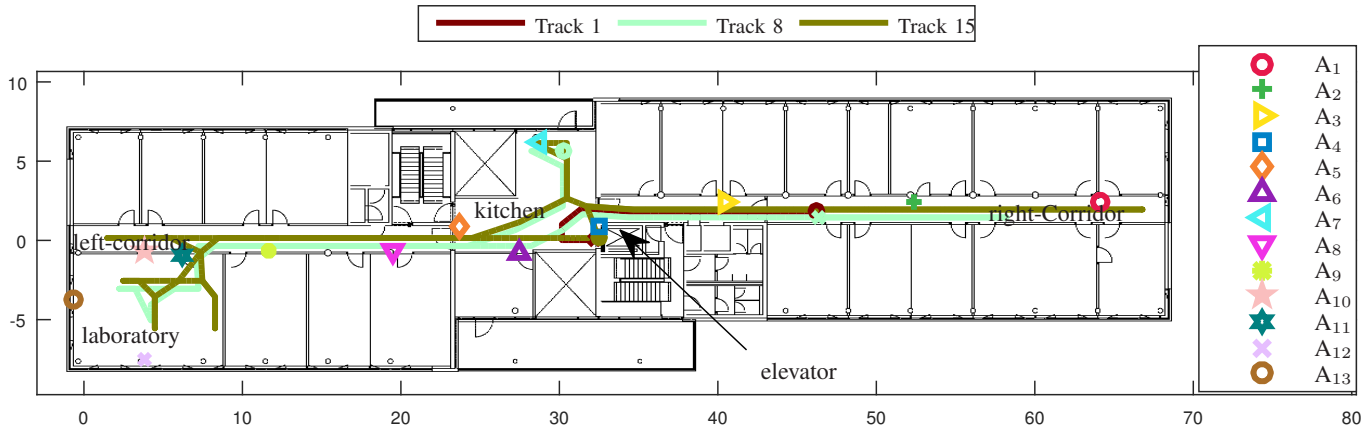

Fig. 5. Measurement scenario with 13 fixed anchors (A_1 to A_{13}) and moving units (pedestrians).

TABLE I
ANCHOR POSITIONS

Anchor	Position
A_1	$(64.1\,\text{m}, 2.5\,\text{m})$
A_2	$(52.3\,\text{m}, 2.5\,\text{m})$
A_3	$(40.5\,\text{m}, 2.5\,\text{m})$
A_4	$(32.5\,\text{m}, 0.9\,\text{m})$
A_5	$(23.6\,\text{m}, 0.8\,\text{m})$
A_6	$(27.4\,\text{m}, -0.8\,\text{m})$
A_7	$(28.7\,\text{m}, 6.1\,\text{m})$
A_8	$(19.5\,\text{m}, -0.7\,\text{m})$
A_9	$(11.7\,\text{m}, -0.7\,\text{m})$
A_{10}	$(3.8\,\text{m}, -0.7\,\text{m})$
A_{11}	$(6.2\,\text{m}, -1.0\,\text{m})$
A_{12}	$(3.7\,\text{m}, -7.6\,\text{m})$
A_{13}	$(-0.6\,\text{m}, -3.7\,\text{m})$

with 13 anchors at positions summarized in Table I. The measurements were conducted on the second floor of an office building. We recorded the UWB and IMU data for 15 independent tracks where different pedestrians carried the hand-held device. Details about the different tracks are summarized in Table II, where the path description summarizes roughly the movement of the pedestrians with K for kitchen, LC for left corridor, RC for right corridor L for laboratory. Three example tracks are indicated in Fig. 5, where the starting position of each track is marked by a cross and the end position by a circle. In order to obtain the ground truth of the moving pedestrians we measured ground truth points (markers) of the track in advance. Whenever the pedestrians walk on such a marker, it was recorded in the data capturing software running on the laptop. By using these ground truth points we obtain an accuracy of the pedestrian location in the order of 20 cm.

Fig. 6 shows three examples of the estimated propagation distances $\hat{d}_{n,i}(t_k)$ for $n \in \{1, 8, 15\}$ in meter versus the pedestrian moving time in seconds. The figures show additionally by the black lines the corresponding calculated propagation distances, which match to the UWB measurements.

The evaluations are performed using $N_s = 2000$ particles in the superPF, whereas the number of particles for the subPFs for each anchor is different depending on the estimated distance and convergence of the anchor positions. The developed algorithm obtains the measurements $\mathbf{z}_n(t_k)$ and the heading rate $\dot{\Psi}_n(t_k)$ every $T = t_k - t_{k-1} = 0.5\,\text{s}$. The error in the heading noise is modeled by a Gaussian density $w_{\Psi,n}(t_k) \sim \mathcal{N}\left(0, \sigma^2_{\Phi}(t_k)\right)$ with standard deviation $\sigma_{\Phi}(t_k) = 1\,^\circ$. As mentioned before, the processing of the Tracks $1-15$ is done sequentially. Hence, the n-th PF (Track n) uses as prior information, the anchor estimations and mapped path of the $n-1$-th PF (Track $n-1$). For the initialization of Tracks 1-5, we use prior information $\mathrm{p}\big(\mathbf{x}_{\mathrm{u},n}(t_0)\big)$ including the starting position and velocity. Track 1-5 start at the elevator which serves as a reference to define the coordinate system. All other tracks are initialized by using a least square (LS) algorithm to obtain the starting position, where the velocity is initialized randomly. The n-th LS algorithm uses the anchor positions estimates from the $n-1$-th PF to calculate the intial mobile unit position. Without prior information on the anchor positions (a distance to an anchor is measured the first time), the PF is initialized solely based on the measured distance. Hence, the possible position of anchor A_i lies on a circle around the current mobile unit position $\boldsymbol{r}_{\mathrm{u},n}(t_0)$ with radius $\hat{d}_{n,i}(t_0)$. During the pedestrian movement the positions of the anchors converge.

Fig. 7 shows a learned map for hexagon radius $0.7\,\text{m}$ and Track 15, where the grey hexagons indicate the estimated path with the highest (particle) weight. In the visited areas, this map reflects the real path and is accurate to about 1-3 m, with better accuracy in the corridors and kitchen that were frequented more often. A sufficient number of hexagons have to be revisited several times for a usable map to emerge. Accuracy in any case is related to the physical structure dimension, such as corridors and doors, which is about 1-2 m.

Fig. 8 shows the PDFs of the estimated anchor positions

TABLE II
DESCRIPTION OF TRACKS

Track	Duration	Start pos.	End pos.	Description
1	26 s	(32 m, 0 m)	(46.1 m, 1.8 m)	K ⇒ RC
2	176 s	(32 m, 0 m)	(32 m, 0 m)	K ⇒ RC ⇒ K ⇒ LC ⇒ L ⇒ LC ⇒ K
3	32 s	(32 m, 0 m)	(7.8 m, −5.7 m)	K ⇒ LC ⇒ L
4	22 s	(32 m, 0 m)	(32 m, 0 m)	K
5	36 s	(32 m, 0 m)	(31.25 m, 2 m)	K ⇒ LC ⇒ K
6	49 s	(32 m, 0 m)	(1 m, 0 m)	K ⇒ LC
7	90 s	(30 m, 6 m)	(32 m, 0 m)	K ⇒ LC ⇒ L ⇒ LC ⇒ K
8	98 s	(34.2 m, 1.8 m)	(15 m, 0 m)	RC ⇒ K ⇒ LC ⇒ L ⇒ LC
9	123 s	(46.1 m, 1.8 m)	(30 m, 6 m)	RC ⇒ K ⇒ LC ⇒ L ⇒ LC ⇒ K ⇒ K
10	78 s	(66.3 m, 1.8 m)	(32 m, 0 m)	RC ⇒ K
11	68 s	(5 m, 0 m)	(5 m, 0 m)	LC ⇒ K ⇒ LC ⇒ L ⇒ LC ⇒
12	75 s	(2 m, −2.7 m)	(66.3 m, 1.8 m)	L ⇒ RC ⇒ K ⇒ RC
13	22 s	(54 m, 1.8 m)	(30 m, 6 m)	RC ⇒ K ⇒ LC ⇒ K
14	45 s	(32 m, 0 m)	(32 m, 0 m)	K
15	204 s	(32 m, 0 m)	(32 m, 0 m)	K ⇒ LC ⇒ L ⇒ LC ⇒ K ⇒ RC ⇒ K

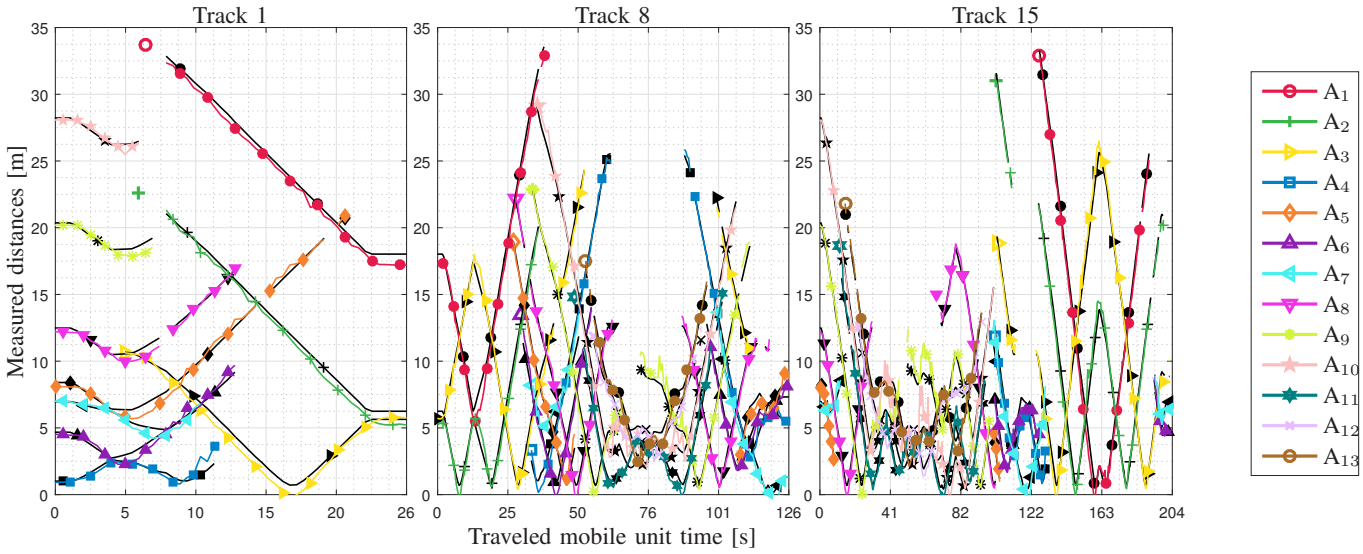

Fig. 6. Recorded delays versus the pedestrian moving time in seconds.

after processing Track 15. Hence, the PDFs of the estimated anchor positions are the estimation results from all 15 tracks. Similar to Fig. 7, we obtain a higher accuracy of the estimated anchor positions in the area which is more frequently visited, i.e. the kitchen where the root mean square errors (RMSEs) of the estimated anchor positions are lower than $0.5\,\mathrm{m}$. Especially, the RMSE of A_7 is below $0.1\,\mathrm{m}$. In the right corridor we can observe that the algorithm is not able to resolve the ambiguities. Two hypotheses of the anchor positions, on both sides of the corridor are equally likely as long as the mobile units move along a straight path. However, as long as the mobile units move on straight paths, like in the corridors, both hypotheses do not influence the mobile units positions estimation results. By turning, the ambiguity can be solved, like entering a room, which is visible in the left corridor when entering the laboratory, where the ambiguities of A_9, A_{10}, A_{11} can be resolved.

V. Conclusions

To conclude, using the developed SLAM algorithm allows building up an UWB indoor positioning system without measuring the locations of the UWB anchors. The UWB anchor positions are dynamically estimated using a iterative SLAM approach using mobile units. Additionally, we propose path mapping that represents the mobile units motion in a two-dimensional hexagonal grid. As soon as the mobile units return

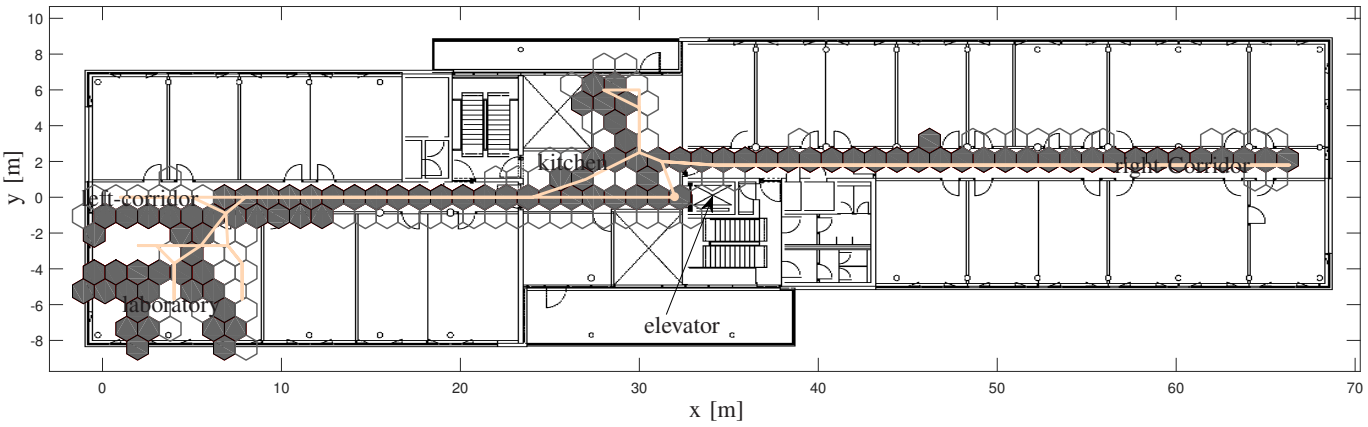

Fig. 7. A learned map for hexagon radius 0.7 m and Track 15: the grey hexagons indicate the estimated path with the highest (particle) weight.

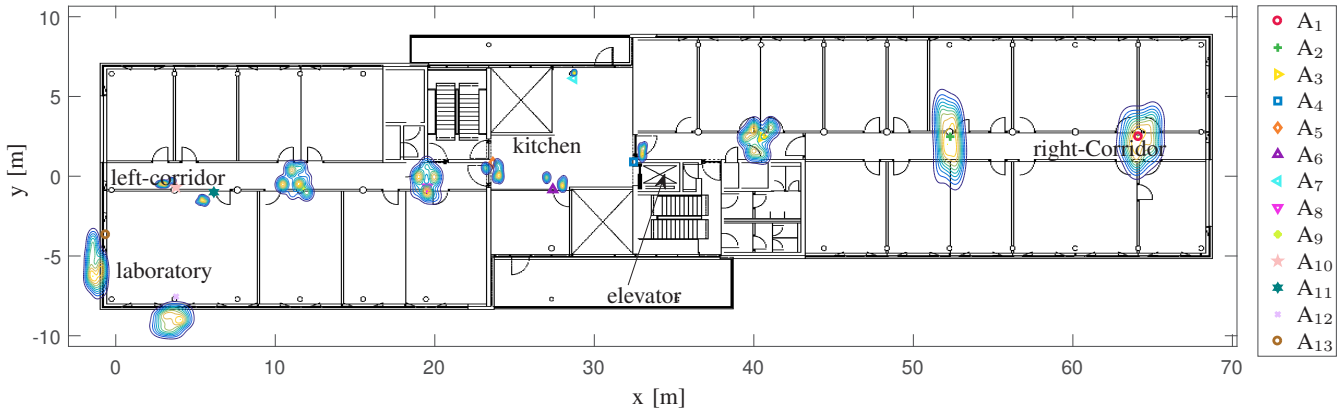

Fig. 8. PDFs of the estimated anchor positions after processing Track 15.

to already mapped positions, information of these positions can be reused to correct for estimation errors. By assigning the mapping task to a group of collaborating mobile units allows to merge the resulting individual mapped paths to generate a more complete and accurate map of the area.

VI. Acknowledgement

This work has been performed in the framework of the DLR project *Navigation 4.0* and the European Unions Horizon 2020 research and innovation programme under grant agreement No. 636537 *HIGHTS (High precision positioning for Cooperative-ITS applications)*.

References

[1] G. Seco-Granados, J. López-Salcedo, D. Jiménez-Baños, and G. López-Risueño, "Challenges in Indoor Global Navigation Satellite Systems," *IEEE Signal Process. Mag.*, vol. 29, no. 2, pp. 108–131, Mar. 2012.

[2] H. Liu, H. Darabi, P. Banerjee, and J. Liu, "Survey of Wireless Indoor Positioning Techniques and Systems," *IEEE Trans. Syst., Man, Cybern. C*, vol. 37, no. 6, pp. 1067–1080, Nov. 2007.

[3] D. Dardari, P. Closas, and P. M. Djuri?, "Indoor Tracking: Theory, Methods, and Technologies," *IEEE Trans. Veh. Technol.*, vol. 64, no. 4, pp. 1263–1278, Apr. 2015.

[4] K. Kaemarungsi and P. Krishnamurthy, "Properties of Indoor Received Signal Strength for WLAN Location Fingerprinting," in *Proc. Int. Conf. on Mobile and Ubiquitous Systems: Computing, Networking and Services*, Aug. 2004, pp. 14–23.

[5] Y. Luo, O. Hoeber, and Y. Chen, "Enhancing Wi-Fi fingerprinting for indoor positioning using human-centric collaborative feedback," *Human-centric Computing and Information Sciences*, vol. 3, no. 1, p. 2, 2013.

[6] P. Bahl and V. N. Padmanabhan, "RADAR: an In-Building RF-Based User Location and Tracking System," in *Proc. IEEE INFOCOM 2000. Conf. on Comp. Commun.*, vol. 2, 2000, pp. 775–784 vol.2.

[7] M. Win and R. Scholtz, "Characterization of Ultra-Wide Bandwidth Wireless Indoor Channels: a Communication-Theoretic View," *IEEE J. Sel. Areas Commun.*, vol. 20, no. 9, pp. 1613–1627, Dec. 2002.

[8] A. Molisch, D. Cassioli, C.-C. Chong, S. Emami, A. Fort, B. Kannan, J. Karedal, J. Kunisch, H. Schantz, K. Siwiak, and M. Win, "A Comprehensive Standardized Model for Ultrawideband Propagation Channels," *IEEE Trans. Antennas Propag.*, vol. 54, no. 11, pp. 3151–3166, Nov. 2006.

[9] C. Steiner and A. Wittneben, "Low Complexity Location Fingerprinting With Generalized UWB Energy Detection Receivers," *IEEE Trans. Signal Process.*, vol. 58, no. 3, pp. 1756–1767, Mar. 2010.

[10] I. Oppermann, M. Hämäläinen, and J. Iinatti, *UWB: Theory and Applications*. John Wiley & Sons, 2005.

[11] G. Shi and Y. Ming, "Survey of Indoor Positioning Systems Based on Ultra-wideband (UWB) Technology," in *Wireless Communications, Networking and Applications*. Springer, 2016, pp. 1269–1278.

[12] H. Liu, H. Darabi, P. Banerjee, and J. Liu, "Survey of Wireless Indoor Positioning Techniques and Systems," *IEEE Transactions on Systems, Man, and Cybernetics, Part C (Applications and Reviews)*, vol. 37, no. 6, pp. 1067–1080, 2007.

[13] S. Lee, B. Kim, H. Kim, R. Ha, and H. Cha, "Inertial sensor-based indoor pedestrian localization with minimum 802.15. 4a configuration," *IEEE Trans. Ind. Informat.*, vol. 7, no. 3, pp. 455–466, 2011.

[14] C. Gentner and M. Ulmschneider, "Simultaneous Localization and Mapping for Pedestrians using Low-Cost Ultra-Wideband System and

Gyroscope," in *Proc. IEEE Int. Conf. on Indoor Positioning and Indoor Navigation*, Saporo, Japan, Sep. 2017.

[15] S. Zhang, E. Staudinger, W. Wang, C. Gentner, A. Dammann, and E. Sandgren, "DiPLoc: Direct signal domain particle filtering for network localization," in *Proceedings of ION GNSS+*. Tampa, Florida, USA: ION, Sep. 2015.

[16] C. Gentner, B. Ma, M. Ulmschneider, T. Jost, and A. Dammann, "Simultaneous Localization and Mapping in Multipath Environments," in *IEEE/ION PLANS*, Savanah, GO, USA, Apr. 2016.

[17] H. Durrant-Whyte and T. Bailey, "Simultaneous Localization and Mapping: Part I," *IEEE Robot. Autom. Mag.*, vol. 13, no. 2, pp. 99–110, Jun. 2006.

[18] T. Bailey and H. Durrant-Whyte, "Simultaneous Localization and Mapping (SLAM): Part II," *IEEE Robot. Autom. Mag.*, vol. 13, no. 3, pp. 108–117, 2006.

[19] C. Gentner, R. Pöhlmann, M. Ulmschneider, T. Jost, and S. Zhang, "Positioning using Terrestrial Multipath Signals and Inertial Sensors," *Mobile Information Systems*, 2017.

[20] P. Robertson, M. Angermann, and B. Krach, "Simultaneous Localization and Mapping for Pedestrians using only FootMounted Inertial Sensors," in *In Proc. UbiComp 2009, ACM*, 2009, pp. 93–96.

[21] M. Angermann and P. Robertson, "FootSLAM: Pedestrian Simultaneous Localization and Mapping Without Exteroceptive Sensors - Hitchhiking on Human Perception and Cognition," *Proceedings of the IEEE*, vol. 100, no. Special Centennial Issue, pp. 1840–1848, May 2012.

[22] M. Puyol, D. Bobkov, P. Robertson, and T. Jost, "Pedestrian Simultaneous Localization and Mapping in Multistory Buildings Using Inertial Sensors," *Intelligent Transportation Systems, IEEE Transactions on*, vol. 15, no. 4, pp. 1714–1727, Aug 2014.

[23] C. Gentner, T. Jost, W. Wang, S. Zhang, A. Dammann, and U.-C. Fiebig, "Multipath Assisted Positioning with Simultaneous Localization and Mapping," *IEEE Trans. Wireless Commun.*, vol. 15, no. 9, pp. 6104–6117, Sep. 2016.